Performance Comparison of Analytical Solutions for bSSFP Signal Demodulation

Michael N Hoff[1], Jalal B Andre[1], and Qing-San Xiang[2]

[1]*Radiology, University of Washington, Seattle, Washington, United States,* [2]*Physics, University of British Columbia, Vancouver, British Columbia, Canada*

Target Audience MRI scientists and biomedical and electical engineers.

Purpose Balanced steady state free precession (bSSFP) sequences efficiently generate high signal images,but magnetic field inhomogeneity yields excessive interpulse phase evolution θ that causes signal nulls (bands) in images. Band attentuation is tyically achieved by combining radiofrequency (RF) phase-cycled bSSFP images[1,2]. We have demonstrated two analytical solutions that demodulate bSSFP of its dependence on θ using four phase-cycled images: 1) a geometric solution GS[3], formed at the crossing of lines connecting data points in the complex plane, and 2) an algebraic solution AS[4], formed using algebraic manipulation. The purpose here is to compare their noise and artifact-correction performance, and propose a hybrid solution that increases the potential for clinical viability.

Methods The complex bSSFP magnetization I_k may be described by Eq.1[5,6] as a function of parameters M, E_2, b and θ, with T_1 and T_2 relaxation terms given by $E_1 = e^{-TR/T_1}$ and $E_2 = e^{-TR/T_2}$, RF flip angle α, and repetition time TR. The AS (Eq. 2) and GS (Eq. 3) are unique formulations of the θ-independent parameter M to be computed with phase-cycled bSSFP images.

$$I_k = M\frac{1-E_2e^{i(\theta+\Delta\theta_k)}}{1-b\cos(\theta+\Delta\theta_k)} \qquad M = \frac{M_0(1-E_1)\sin\alpha}{1-E_1\cos\alpha-E_2^2(E_1-\cos\alpha)} \qquad b = \frac{E_2(1-E_1)(1+\cos\alpha)}{1-E_1\cos\alpha-E_2^2(E_1-\cos\alpha)} \quad (1)$$

AS
$$M = \frac{I_1I_3(I_2-I_4)(1+i)+I_2I_4(I_1-I_3)(1-i)}{I_1I_2-I_3I_4+i(I_2I_3-I_1I_4)} \quad (2)$$

GS
$$M = \frac{(x_1y_3-x_3y_1)(I_2-I_4)-(x_2y_4-x_4y_2)(I_1-I_3)}{(x_1-x_3)(y_2-y_4)+(x_2-x_4)(y_3-y_1)} \quad (3)$$

GAS
$$M_{GAS} = M_{AS}W_{AS} + M_{GS}W_{GS} \qquad W_{AS} = \frac{V_{GS}}{V_{AS}+V_{GS}} \qquad W_{GS} = 1 - W_{AS} \quad (4)$$

TRE
$$\sigma = \frac{\sqrt{\sum_{x,y}[I_w(x,y)-|I_{xs}(x,y)|]^2}}{\sum_{x,y}|I_{xs}(x,y)|} \quad (5)$$

All data was simulated/acquired with $k = 1 \rightarrow 4$ images respectively RF phase cycled at $\Delta\theta_k = 0°$, 90°, 180°, and 270°. Simulated data employed α = 41°, TR = 5ms, E_2 varied from 0.9 → 0.9999 horizontally and b varied from 0.1 → 0.8 vertically (to emulate typical tissue T_1 and T_2 values), and θ varied from –π to π (Fig.1a-d). *In vivo* images were acquired on a 3T Philips Ingenia scanner with α = 36°, TR/TE = 4.5/2.25ms, 256/192/176 matrix size and 1.09/1.09/2mm voxel size along frequency/phase/slice directions (Fig.2a shows $\Delta\theta$ =180° image).

The complex sum (CS), GS, AS, and a hybrid Geometric-Algebraic Solution (GAS) were computed pixel-by-pixel on all data. $k = 1 \rightarrow 4$ complex signal values I_k, real parts x_k, and imaginary parts y_k were input into Eq.2 and Eq.3 for the GS and AS respectively; their regional variances V_{GS} and V_{AS} were then employed to form a minimal-variance GAS image using Eq. 4. The total relative error (TRE) for each technique relative to their gold standards (M for the GS, AS, and GAS, and the centre of mass for the CS[3]) was computed on simulated data using Eq. 5.

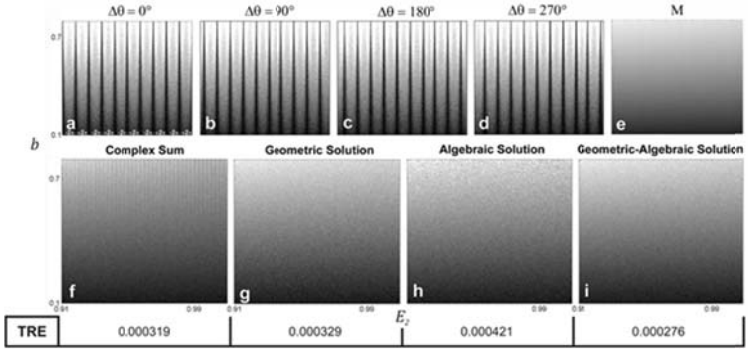

Fig.1: Simulated bSSFP signal demodulation. a-d. Phase cycled magnitude images. e. Gold standard *M* image. f. Complex sum, g. geometric solution, h. algebraic solution, and i. geometric-algebraic solution of a-d. TRE values given.

Results Fig. 1 indicates that the GS, AS, and GAS eliminate banding and signal modulation, while the CS sometimes has residual banding with a four-fold spatial frequency increase. The AS is relatively unstable in higher signal/b-value regions, while the GAS achieves the lowest TRE by ameliorating regional instabilities of the GS and AS. Green arrows in Fig. 2 indicate that the GS, AS, and GAS all correct banding in *in vivo* bSSFP images, while the CS does not. Deficiencies in the image quality seen in the GS and AS are predominately overcome by the GAS. The Fig. 3a plot of reconstruction TRE vs. variable bSSFP image noise shows finite error in the CS even without image noise. Error increases gradually for the CS and steeply for the AS with increased noise level, while the GAS always yields the least error. The Fig. 3b plot of TRE vs. variable T_1/T_2 ratio indicates high AS and CS error at small T_1/T_2 ratio, while the GAS has consistently lower TRE than the GS and AS.

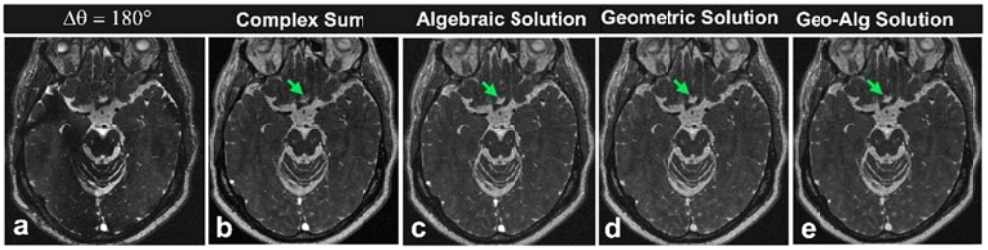

Fig.2: bSSFP suprasellar cistern region demodulation. a. 1 of 4 phase-cycled magnitude images. b. Complex sum, c. algebraic solution, d. geometric solution, and e. geometric-algebraic solution of the four phase cycles. Arrows indicate that c, d, and e correct residual banding remnant in the complex sum.

Discussion The GS and AS respond uniquely to noisy data; coupled with the GS' ability and AS' inability to function following swapping of input real and imaginary parts, this suggests that they are fundamentally different solutions. The AS' many multiplicative operations yield large error propagation for strong signal/low T_1/T_2 regions, but at relatively high T_1/T_2 ratio it performs similarly to if not better than the GS. The GAS exploits the regional strengths of the GS and AS to generate a variance-minimized combination with comparable or less error than the CS, without the banding that the CS can exhibit. The existence of two unique analytical solutions suggest that similar artifact correction should be possible with less data.

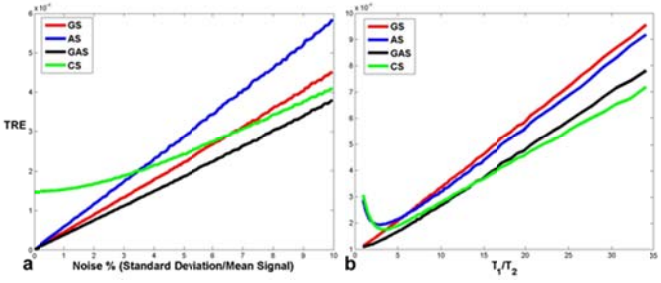

Fig.3: The TRE of the geometric solution (GS), algebraic solution (AS), geometric-algebraic Solution (GAS), and complex sum (CS) are plotted as a function of a) variable noise and b) T_1/T_2 ratio.

Conclusion While the GS and AS perform uniquely in noise, the GAS for bSSFP signal demodulation exploits their strengths to achieve an mvariance solution.

References 1. Zur *et al*., MRM, 16:444-459, 1990. 2. Bangerter *et al*., MRM, 51:1038-1047, 2004. 3. Xiang QS & Hoff MN, MRM, 71:927-933, 2014. 4. Hoff & Xiang, Proc. ISMRM, 19: 2824, 2011. 5. Ernst & Anderson, Rev Sci Instrum, 37:93-102, 1966. 6. Lauzon & Frayne, Conc Mag Res, 34A(3):133-143, 2009.